Journal of Molecular Structure 1282 (2023) 135141

Contents lists available at ScienceDirect

Journal of Molecular Structure

journal homepage: www.elsevier.com/locate/molstr

Novel copper (II) and zinc (II) complexes with enrofloxacin and oxolinic acid: synthesis, characterization, Hirshfeld surface and DFT/CAM-B3LYPD3BJ studies: NBO, QTAIM and RDG analysis

Amina Boughougal[a], Rayene Kadri[b], Mekki Kadri[b,*], Jean Bernard Tommasino[c], Guillaume Pilet[c], Amel Messai[a], Dominique Luneau[c]

[a] Laboratory of Engineering and Advanced Materials Science (ISMA), Abbes Laghrour University, Khenchela, 40000, Algeria
[b] Laboratoire de Chimie Physique, Université 8 Mai 1945, BP401, Guelma 24000, Algérie
[c] Laboratoire des Multimatériaux et Interfaces UMR 5615, CNRS, Université Claude Bernard, Lyon. 1, avenue du 11 novembre 1918, 69622 Villeurbanne Cedex, France

ARTICLE INFO

Article history:
Received 29 November 2022
Revised 4 February 2023
Accepted 9 February 2023
Available online 15 February 2023

Keywords:
Enrofloxacin
oxolinic acid
metallic complexes
DFT

ABSTRACT

This study aimed to investigate the crystal structure of the synthesized complexes of Cu (II) and Zn (II) with enrofloxacin and oxolinic acid. The characterization of the complexes was carried out using single–crystal x-ray diffraction, Hirshfeld surface and ^{1}H NMR spectroscopy. In addition, a DFT/6-31g(d) investigation was conducted to assess the performance of two exchange-correlation functionals CAM-B3LYP and CAM-B3LYPD3BJ to predict both covalent and non-covalent bonds lengths, and the vibrational frequencies of the metallic complexes.

The main findings of this study indicate that the interaction between each metallic ion and the corresponding ligand leads to significant modifications in bond lengths, Mulliken charge distribution and electrostatic potential values in the complex molecules as compared to the ligands alone. To gain further insights into these complexes, several calculations were performed, such as Natural Atomic orbitals (NAO), Natural Bond orbitals (NBO), and Quantum Theory of Atoms in Molecules (QTAIM) analysis. The non-covalent interactions were explored and visualized in two and three-dimensional spaces with the help of the Reduced electron Density Gradient (RDG) approach.

1. Introduction

The transition metal complexes are essential to human metabolism. There are some examples of coordination compounds present in living organisms such as coenzyme B12, chlorophyll and hemoglobin [1]. In therapeutic domain, the metalloantibiotic entities are largely known to interact with different bacteria types with a synergic effect. Therefore, metallo-antibiotic complexes have been significantly active over the past years because of the wide variety of possible ligand structures determined by the family of antibiotics used. For example, the commercial silver sulfadiazine complex is known for the treatment of burns. Others metallo-antibiotic complexes were synthesized and characterized with an improving of the biological response.

Recently, we have demonstrated that the strategy of nosocomial treatment using a cocktail of complementary antibiotics can be improved through coordination chemistry [2]. A new model complex was synthesized and characterized, which consists of two different antibiotic ligands (sulfonamide and quinolone) linked to a zinc metal ion. This model showed surprising biological effectiveness against E. coli, S. Aureus, and E.Faecalis. Based on these results, modifying the physicochemical parameters of the ligand in the complex seems to be a good approach to explain the synergistic effect

Among others ligands, special attention were paid to the quinolones because the molecular structures of their metal complexes display many coordination modes. For instance, the keto-carboxylic acids found in quinolone and fluoroquinolone complexes give many molecular structures with bidentate or tridentate binding modes due to the presence of a piperazine group [3]. Furthermore, the inhibition of the DNA-Gyrase in the bacteria by quinolone species is poorly known [4,5] and a theoretical approach by comparison of quinolone ligand and complex associated to biologic effect offers a new lead to explore the relationship between structure and activity.

* Corresponding author Tel: +213698080567
E-mail address: mekkadri@gmail.com (M. Kadri).

https://doi.org/10.1016/j.molstruc.2023.135141
0022-2860/

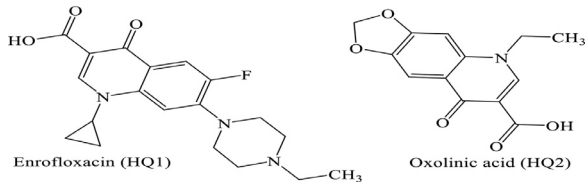

Fig. 1. Chemical structures of ligands used in this work.

A literature review showed that metal complexes of enrofloxacin (HQ1) or oxolinic acid (HQ2) (Fig. 1) have been obtained by several synthetic methods [6–23]. Unfortunately, the obtained complexes are mixed derivatives, in the sense that in addition of the initial ligands HQ1 or HQ2 they include in their structures co-ligands, such as phenanthroline in complex $[Zn(erx)_2(py)_2].6H_2O$ [24] or 2,2 bipyridine in [(Cu(oxo) (phen)Cl] [25].

In continuation of our previous works [2,34], this paper describes the synthesis and the characterization of HQ1/Cu(II) and HQ2/ Zn(II) complexes. Their crystal structures without co-ligand represented as $[Cu(Q1)_2\ H_2O].6H_2O$ and $[Zn(Q2)_2\ H_2O].3H_2O$ were characterized by a single–crystal X-ray diffraction, Hirshfeld surface and ^1H NMR spectroscopy.

To gain further insights into the structure and properties of the studied complexes, the work was complemented with a study at DFT level. Firstly, the performance of two selected exchange-correlation functionals CAM-B3LYP and CAM-B3LYPD3BJ was assessed to predict both covalent and non covalent bonds in the copper complex molecule. The first selected level is an hybrid- exchange-correlation functional based on the Coulomb – attenuation method [26]. The second one is the same exchange functional but additionally includes the Grimme's dispersion correction of type D3BJ (D3 with Becke-Johnson damping) [27].

The best performing DFT/6-31g(d) level so selected will be used in further calculations such as the prediction of the Mulliken charges, Molecular Electrostatic Potential (MEP), vibrational frequencies, and global reactivity parameters.

The nature and the strength of the interaction between the reactants was studied with natural atomic orbital (NAO), natural bond orbital (NBO) and the quantum theory of atoms in molecules (QTAIM) analysis.

In addition, non covalent interactions developed in $[Cu(Q1)_2H_2O].6H_2O$ and $[Zn(Q2)_2H_2O].4H_2O$ systems were explored and visualized in two and three-dimensional spaces using the reduced electron density gradient (RDG) technique.

2. Experimental section and computational details

2.1. Materials

All chemicals (enrofloxacin, oxolinic acid, $CuCl_2$, Zn $(ClO_4)_2.6H_2O$ and all solvents NH_3, CH_3OH, DMSO were purchased from Sigma-Aldrich.

These chemicals and solvents were reagent grade and were used as purchased.

2.2. Chemical measurements

2.2.1. X-ray diffraction

Single-crystal X-ray studies of metallic complexes were carried out using a Gemini diffractometer and related analysis software [28]. An absorption correction based on the crystal faces was applied to the data sets (analytical) [29,30].

The structures were solved using direct methods with the SIR97 program [31], combined with Fourier difference syntheses, and refined against F using reflections with $[I/\sigma(I) > 3]$, by using the CRYSTALS program [32]. All atomic displacement parameters for non-hydrogen atoms were refined using anisotropic terms. The hydrogen atoms were theoretically located based on the conformation of the supporting atom and refined using the riding model. Data collection, structure refinement parameters, and crystallographic data for the complexes are indicated in Table S1 (Supplementary Materials). The Cambridge Crystallographic Data Centre (CCDC) provides additional crystallographic data used in the experiments, accessible through their website (www.ccdc.cam.ac.uk/structures). The data, stored in CCDC codes 2191391 and 2191392, is available for free.

2.2.2. Hirshfeld surface analysis

The Hirshfeld Surfaces (HSs) and their related 2D-fingerprint plots (FPs) were obtained using Crystal Explorer 21 software [33]. The HS was mapped over $d_{norm,}$ shape index and the curvedness functions of the studied structures, respectively in the range of [-0.6750 to 1.3099Å], [-1.000 to 1.000Å] and [−4.000 to 0.4000 Å] for the zinc complex, and [-0.1712 to 2.8428 Å], [-1.000 to 1.000Å] and [−4.000 to 0.4000 Å] for the copper complex.

2.2.3. NMR spectroscopy

^1H NMR spectroscopy were performed on a 400 MHz ADVANCE III HD NMR, equipped with a 5 MM diameter BBO probe using the dimethyl sulfoxide (DMSO) as a solvent and tetramethylsilane as an internal reference. MestReNova software was used to visualize and calculate the parameters (integrals, peaks) of the ^1H NMR spectra.

2.2.4. Infrared spectroscopy

FTIR spectra were performed from 4000 to 400 cm^{-1} with a Nicolet 380 FTIR spectrometer coupled with the attenuated total reflectance (ATR) accessory.

2.2.5. Synthesis of the complexes

The complexes were synthesized according to the method described earlier [2,34]**.** A solid mixture of the metal salt 1 mmol ($CuCl_2$ and Zn $(ClO_4)_2.6H_2O$) with two equivalents of ligand HQ1 and oxolinic acid HQ2 dissolved in 5 ml of methanol. The drop wise of a concentrated ammonia solution (25%) was then introduced until a blue limpid solution for Cu (II) and a white limpid solution for the Zn (II) were obtained. After a week of slow evaporation of the solvent at room temperature, single-crystals were recovered by filtration with a 29% yield of copper complex and a 67% yield of zinc complex.

2.3. Computational details

Molecular modeling calculations were performed using GAUSSIAN 09 software [35] at DFT/6-31g(d) level, using CAM-B3LYP and CAM-B3LYP D3BJ exchange-correlation functionals.

The optimized structures were checked as minima on the potential energy surfaces by frequency calculations. The highest occupied molecular orbital (HOMO), the lowest unoccupied molecular orbital (LUMO) and the optimized structures were visualized with GaussView [36]. Vibrational harmonic frequency analysis was used to ensure that it is a truly local minimum having no imaginary frequencies.

3. Result and discussion

3.1. Crystal structure description of Cu(II) complex

The copper complex crystallizes in the triclinic space group *P-1*. The unit cell parameters are: a=12.1323(4) Å, b=13.3585(6) Å, c=16.0606(6) Å, α=111.727(4) º, β=92.956(3) º and γ=113.194(3)

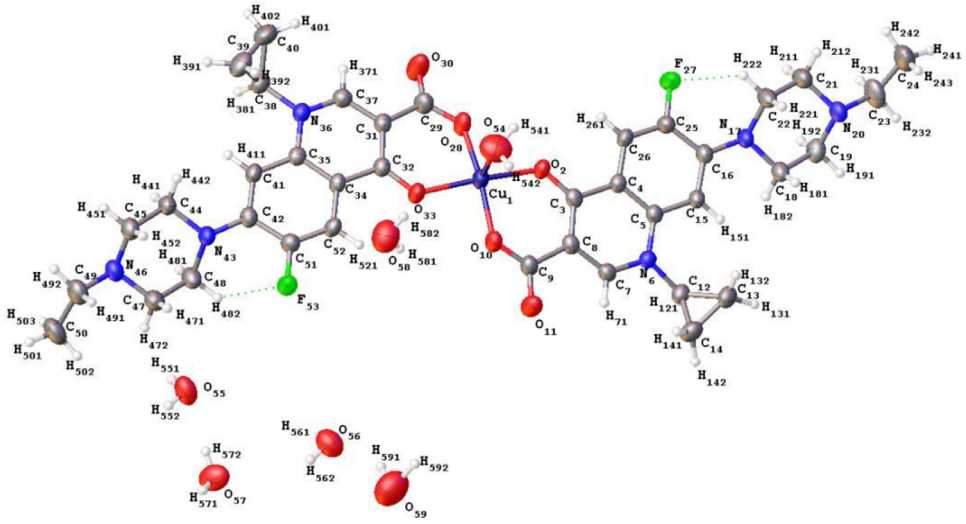

Fig. 2. View of the asymmetric unit of the Cu (II) complex.

º. An ORTEP diagram with thermal ellipsoids drawn at 50% probability level is depicted in Fig. 2. This diagram illustrate the asymmetric unit of copper complex is depicted in

A short intermolecular C22–H221…F27 and C48–H481…F53 hydrogen bonds interactions with a distances of 2.142 Å and 2.250 Å respectively, this interactions formed a *S(6)* ring motif [37] which plays a critical role in the stabilization of crystal structure [38,39].

Each Cu (II) ion is bound with two deprotonated bidentate ligands (Q1) and one water molecule. The ion-ligand interactions were established via five oxygen donor atoms: Cu-O2, Cu-O10, Cu-O28, Cu-O33 and Cu-O54 with bond lengths 1.935, 1.928 Å, 1.935 and 1.944 Å and 2.212 Å, respectively.

The distortions from a square-based pyramid to a trigonal bipyramid geometry around the copper ion were determined by using Addison's parameter τ as a measure of the degree of trigonality (τ = 0.13) revealing a distorted square-based pyramid shape [40].

The two piperazine rings in the complex molecule (N17–C22–C21–N20–C19–C18) and (N43–C44–C45–N46-C47–C48) were non-planar. The atoms (N17, C19, C21) and (N43, C45, C47) were located above the plane, however (C22, C18, N20) and (C44, C48, N46) under the plane.

The crystal structure is stabilized by O–H···O hydrogen bond interactions which are listed in Table S2 and Fig. S1$_a$ (Supplementary Materials). These hydrogen bonds give rise to the ring- graph-motifs $R_2^3(8)$ and $R_4^4(12)$ as displayed in Fig. S1$_b$ (Supplementary Materials).

The copper complex lattice was displayed also a short interaction bonds H···π (O) interactions: C14–H142···π (O2=C) and C14–H142···π (O28=C) with 2.474 Å and 2.731Å, respectively and C24–H241···π(O54) with 2.622 Å distances Fig. S1$_c$ (Supplementary Materials).

In addition we observed the presence of non–covalent π···π stacking interaction as the centroid-to-centroid of pyridine and phenyl rings with the distance of 3.566 Å. This reflects the formation of extra-supramolecular interactions, as highlighted in Fig. S1$_d$ (Supplementary Materials).

3.2. Crystal structure description of Zn(II) complex

Zn(II) complex crystallizes in the orthorombic *Pbca* space group with the unit cell parameters a=19.2883(9) Å, b=7.2672(4) Å, c=21.1817(10) Å. α=90º, β=90 º and γ=90º. The ORTEP diagram with thermal ellipsoids drawn at 50% probability illustrating the asymmetric unit of zinc complex is shown in Fig. S2 (Supplementary Materials). This complex has a monomeric structure of stoichiometry 1 : 2 where the Zn(II) ion is bound to each bidentate ligand (Q2) through the oxygen atom of the carbonyl group and that of the carboxylic group.

In addition, the zinc atom has five coordination sites and can be described as having a distorted square pyramidal geometry. The value of τ = (170.12 - 127.76) / 60 = 0.706 [40], which indicates a distortion of the pyramidal geometry. In the equatorial plane, the positions were occupied by two carboxylic oxygen atoms (Zn-O2 and Zn-O34 with the same bond lengths 1.947 Å) and two oxygen atoms of the carbonyl groups (Zn-O7 and Zn-O39 with bond length 2.099). The water oxygen atom is coordinate on the apical position (Zn-O21= 2.020 Å)

The zinc complex is stabilized by three- dimensional O–H···O hydrogen bonding network (Table S3 and Fig. S3$_a$ in Supplementary Materials). This hydrogen bonds give rise to the rings $R_2^3(10)$ graph-set motif as displayed in Fig. S3$_b$ (Supplementary Materials).

The molecules in individual parallel one-dimensional chains are in contact with the partner molecule belonging to the neighboring chains by π-stacking interactions; the presence of non–covalent π…π stacking interactions as the centroid-to-centroid separation ranges from 3.710 Å to 3.717 Å with molecule chains in the above between phenyl rings···phenyl rings and pyridine···dioxolane rings through, respectively, and around 3.561 Å with molecule chains at the bottom between benzene rings···pyridine rings (Fig. S3$_c$ in Supplementary Materials) .

3.3. Hirshfeld surface analysis

The crystal structure packing of each of the studied complexes was analyzed using the Hirshfeld surface (HS) and associated 2D-fingerprint plots (FPs) generated by the Crystal Explorer package [19,36,39,41,42]. Each point on the HS is defined by two distances (d_e, d_i) with d_e being the distance from the points on the surface to the nearest external nucleus and d_i the distance to the nearest internal nucleus. The normalized contact distance (d_{norm}) based on d_e and d_i can be calculated knowing the van der Waals (vdW) radii of the appropriate atoms internal (d_i^{vdW}) or external to the surface (d_e^{vdW}).

The HSs shown in Fig. S4 and Fig. S5 (Supplementary Materials) were mapped with the normalized contact distance d_{norm}, shape index and curvedness. The d_{norm} reflects the presence of

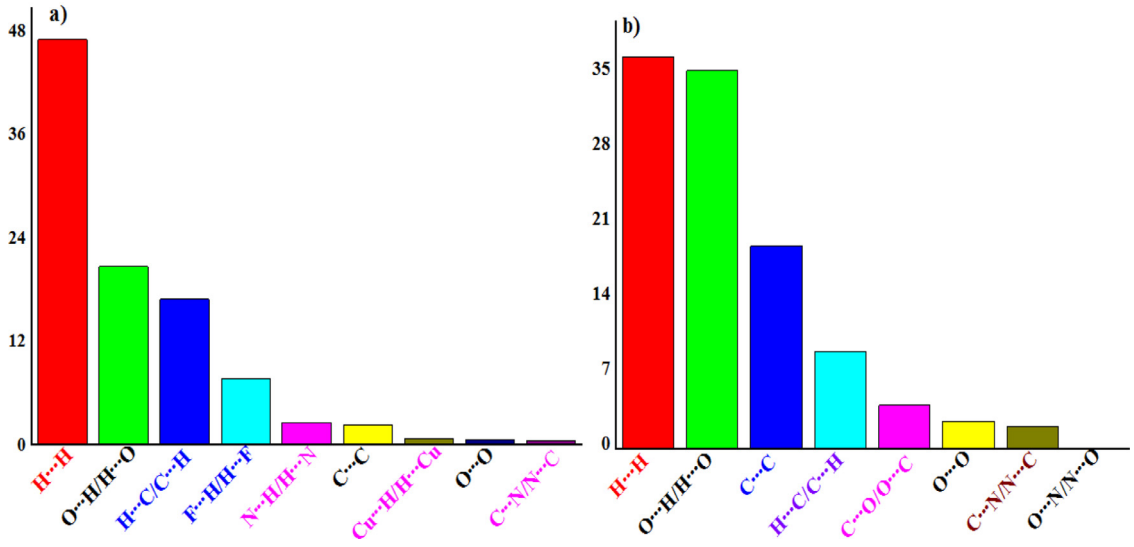

Fig. 3. The percentage contributions of the different molecular contacts in the structures of a) Cu(II) complex and b) Zn(II) complex.

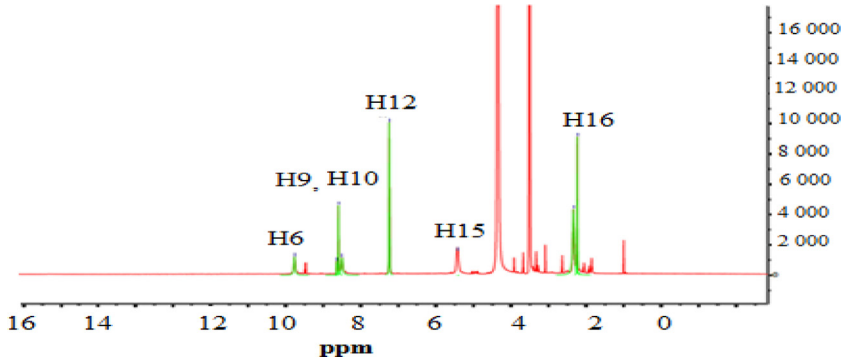

Fig. 4. ^{1}H-NMR spectrum of zinc complex in DMSO.

seven small and big red-spots in copper complex and ten spots in zinc complex. The large red spots indicate the presence of H···O and H···N hydrogen bonds in copper complex and H···O hydrogen bonds in zinc complex on the surface, only with polar H of water molecules. On the other hand, the small spots are associated with the formation of C–H···π interactions. Notably, the weak $\pi\cdots\pi$ stacking interaction can be explored by plotting HS over shape index. The shape index reflects the presence of red and blue triangle-shaped regions around of the aromatic rings on the surfaces of the molecules, indicating the presence of $\pi\cdots\pi$ stacking interactions in the crystal package in both complexes [43,44].

The spikes observed in fingerprint plots [45] Fig. S6 and Fig. S7 (Supplementary Materials) reveal the predominance of H···H (47%) and H···O/O···H (20.7%) intermolecular interactions in the crystal structure of copper complex . In zinc complex, these same interactions account for 36.7% and 35.4% of the surface, respectively. Additionally, two other important contributions are found: C···H/H···C (16.9%) in copper complex and C···C (19%) in zinc complex. Other small contributions (<10%) are observed in interactions (Fig. 3) such as F···H/H···F, N···H/H···N, Cu···H/H···Cu, O···O, C···N/N···C and O···N/N···O.

3.4. ^{1}H-NMR Spectroscopy

Upon the interaction of the ligand with the metallic ion, the ^{1}H-NMR spectrum of the resulting zinc complex in DMSO, as shown in Fig. 4, is different from the spectrum of the ligand, HQ2, which can be found in Fig. S8 (Supplementary Materials).

In the ^{1}H-NMR spectrum of the ligand, the peak located at 15.69 ppm attributed to the acid proton of the carboxylic group disappeared in the spectrum of the complex indicating the deprotonation of the ligand during the interaction.

On the other hand, the protons H6, H10 and H9, H12, H15, H16 of the ligand appear at 8.90, 7.59, 6.30, 4.54, 1.38 ppm, respectively, while in the zinc complex they shift to 8.75, 7.64, 6.24, 4.44 and 1.22 ppm, respectively. These findings characterize the effect of zinc in the molecule, confirming the stability of the complex in solution and the conformational rearrangement.

3.5. Modeling studies

3.5.1. Performance of the exchange functionals in the bond lengths prediction

The bond lengths values of the copper complex predicted by the two selected exchange–correlation functionals, in comparison with the XRD data, are listed in Table S4 (Supplementary Materials).

These results are valuable in evaluating the performance of the selected exchange functionals in predicting structural parameters of copper complex. The connection between the theoretical and experimental results for bond lengths illustrated in Fig. 5 was expressed by the Root Mean Square Error (RMSE).

The CAM-B3LYP exchange functional performed better (RMSE =0.012 Å) than the CAM-B3LYPD3BJ version (RMSE= 0.015 Å) in predicting covalent bond lengths in the complex inner sphere. For

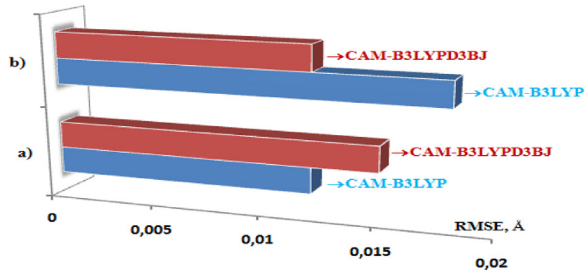

Fig. 5. RMSE values of the bond lengths prediction in a) the inner sphere and b) the inner and the outer spheres.

example, in the prediction of the length of C24 C23 bond, the deviations were 0.020 Å (CAM-B3LYP) and 0.023 Å (CAM-B3LYPD3BJ).

However, the bond lengths between the copper and the oxygen atoms of H_2O in the inner sphere, Cu1O54 and Cu1O58, deviated by -0.058 Å and 0.098 Å, respectively, when calculated using the CAM- B3LYP exchange functional. The deviations were 0.040 Å and -0.006 Å when calculated using the CAM-B3LYPD3BJ level. The same trend was observed in the predictions of the bond lengths between the inner and outer sphere atoms, where the bond are non- covalent. The inclusion of the dispersion correction significantly improved the results. As shown in Fig. 5 (b), the prediction accuracy was improved significantly and CAM-B3LYPD3BJ became the best performing exchange functional.

3.5.2. Complexes structures, Mullikan charges and MEP

The configurations of the Cu(II) and Zn(II) complexes obtained from CAM-B3LYP D3BJ /6-31g(d) level are displayed in Fig. 6 and Fig. S9 (Supplementary Materials**)**. In the first complex, the metal ion is placed between two ligand molecules (stoichiometry 1:2) located in two different planes with a dihedral angle of 143°. In the zinc complex the respective planes of the two ligands were arranged in a T-shape.

According to Werner's conception, the metallic complexes can be represented by the formulas the formulas $[Cu(Q1)_2H_2O].6H_2O$ and $[Zn(Q2)_2H_2O].4H_2O$. One of the water molecules that helps to stabilize each complex can be considered to be located in the inner sphere, as it is significantly closer to the metal ion compared to the other molecules waters. As a result, the bond lengths between Cu-O54 and Zn-O21 are only 2.216 Å and 2.021 Å, respectively.

The values of the distances between oxygen or hydrogen atoms of the water molecules and other atoms of the complexes Table 1 are appropriate for non-covalent interactions formation.

Another interesting observation regarding the variation of the Mulliken during the formation of the complex deserves mentioning. As depicted in Fig. 7, the sites closest to the metallic ion were the most affected following the formation of the copper complex. Additionally, since the complex has a 1:2 stoichiometry, the changes in the charge of the atoms in the two ligands did not occur in the same manner. Thus, in the first ligand molecule Q1a, the most affected atoms were O10, O2 and their neighboring C3 and C9 atoms with charges equal to -0.688e, -0.609e, +0.450e and -0.637e, respectively. However, in the second ligand molecule Q1b, due to the presence of water molecules, the corresponding atoms carried the charges of -0.631e (O28), -0.633(O33), +0.446e (C32) and +0.657e (C29). The nitrogen charge (N17) in Q2a was nearly the same as in the free ligand (-0.503e). However, the charge of the equivalent nitrogen (N43) in Q1b part, underwent a significant change (-0.555e), likely due to the hydrogen bond formation N43···H111 with a length of 1.9810 Å.

Similarly, in the free ligand (HQ2), the atoms O34, O39, C35 and C38 carried the charges of -0.55011e, -0.5022e, 0.5474 e and 0.3942e, respectively. However, in the zinc complex, the charges of the corresponding atoms became -0.6799e, -0.6344e, 0.6086e and 0.4325e in the first ligand molecule (Q2a) and -0.6799e, -0.6693e, 0.6371e, 0.4325e in the second ligand (Q2b). The changes in charges following the formation of the complex are depicted in Fig. 8.

The three dimensional representations of the Molecular Electrostatic Potential (MEP), allowed the visualization of the nucleophilic and electrophilic regions [46] in the ligands (HQ1, HQ2) and in the metallic complexes molecules. From Fig. 9, the most negative potential was over the carbonyl groups of the hydroquinolinic part (C5-O6 and C3-O14), while the most positive region was over the hydrogen atoms (H48 and H30). The electrostatic potential values were changed from -0.108 to + 0.108 a.u.

When the ligands HQ1 and HQ2 interact with copper and zinc ions, respectively, the MEPs of the corresponding complexes showed changes compared to the free ligands maps (Fig. 9). The observed red color on the carbonyl oxygen became more intense, while the intense blue color disappeared. In other words, the range the electrostatic potential values in the free ligands molecules was different from that in the corresponding molecule complex. Therefore, in the HQ1 and HQ2, the MEP values changed from -0.108a.u. to +0.108 a.u., but in the metallic complexes, the new range were -0.119 a.u. to +0.119 a.u., and -0.077 a.u. to +0.077 a.u.

3.5.3. Prediction of the FTIR spectra

The prediction of the main vibration frequencies of the organometallic complexes were carried out at CAM-B3LYPD3BJ level. According to Fig. 10 and Fig. S10 (Supplementary Materials**)** the predicted and experimental spectra of the copper and zinc were in good agreement.

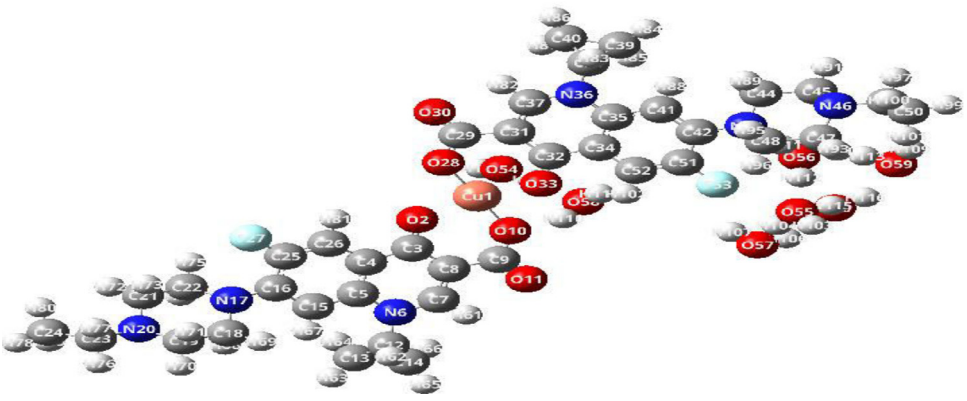

Fig. 6. The optimized structure of copper complex at CAM-B3LYPD3BJ /6-31g (d) level with labels and atomic numbering.

Table 1
Bond lengths (in Å) between ligand atoms and H or O atoms of water molecules.

Cu1-O54	O10-H110	F53-H104	N43-H111	Zn1-O21	O4-H68	O2-H67	H71-O63
2.216	1.809	2.928	1.981	2.020	2.961	1.834	1.723

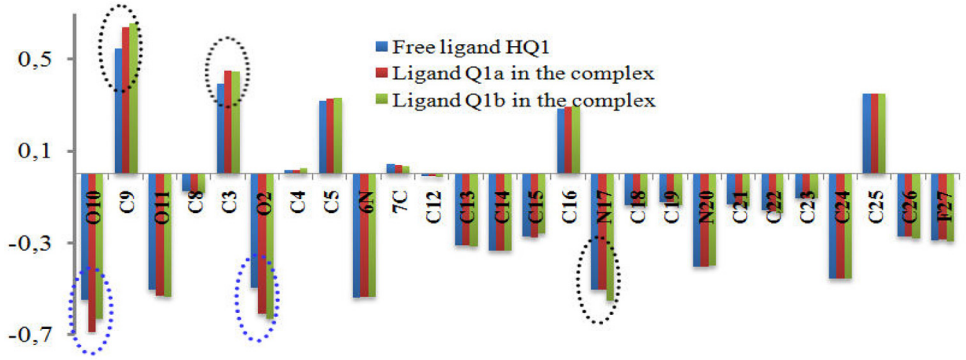

Fig. 7. Atomic charges in the free ligand HQ1 and in Cu(II) complex (Q1a, Q1b).

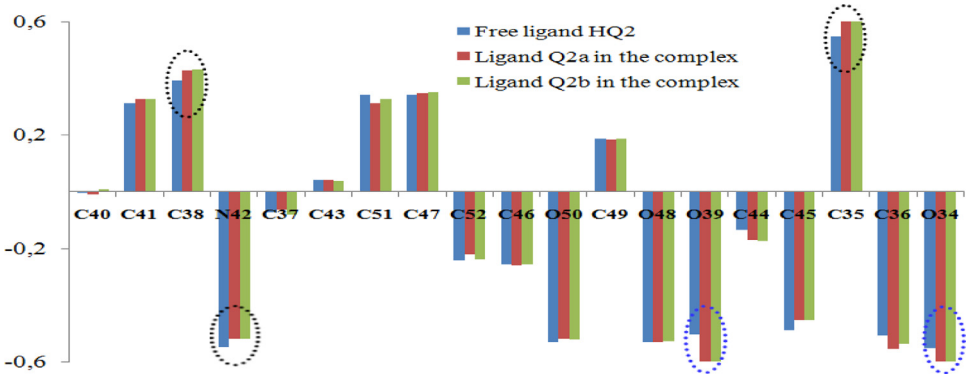

Fig. 8. Atomic charges in the free ligand HQ2 and in Zn(II) complex (Q2a, Q2b).

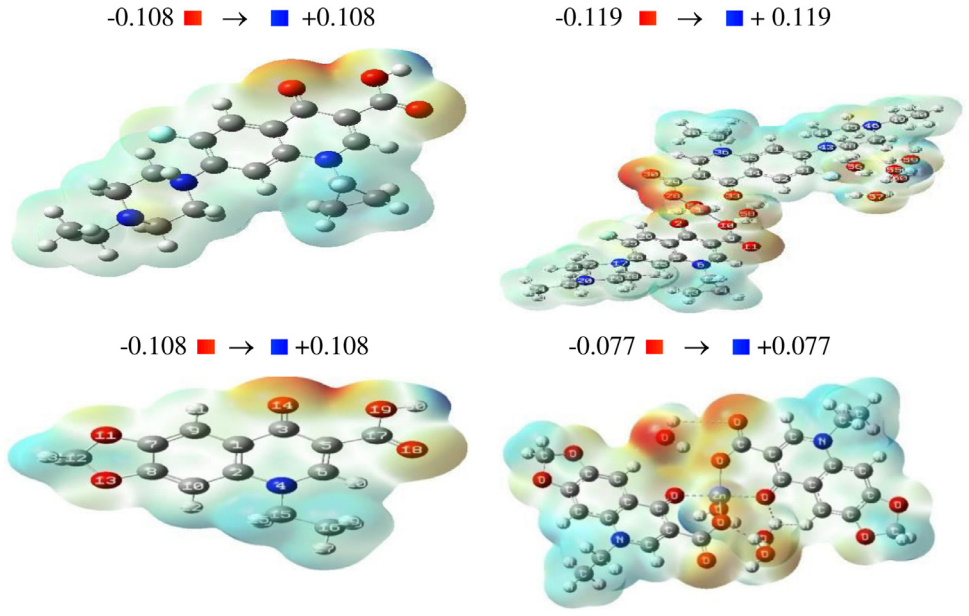

Fig. 9. MEP surfaces calculated at CAM-B3LYPD3BJ /6-31g (d) level for the ligands (HQ1, HQ2) and their corresponding complexes.

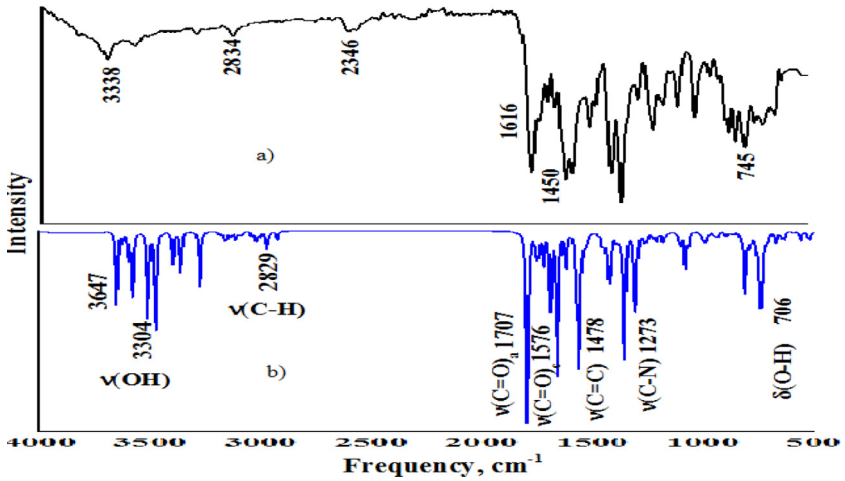

Fig. 10. Comparison of (a) experimental and (b) predicted FTIR spectra of Cu(II) complex.

In the theoretical spectra, the characteristic bands of the (C=O) group were observed at 1707 and 1576 cm^{-1} for the copper complex and 1610 cm^{-1} for the zinc complex. However, the corresponding experimental values were 1616, 1450 and 1578 cm^{-1}, respectively.

The calculated wavenumbers were slightly higher than the values observed for the majority of the normal modes. Two factors may be responsible for the discrepancy between the experimental and calculated spectra of this compound. The first reason is due to the environment and the second one is due to the fact that the experimental value is an anharmonic wavenumber, while the calculated value is a harmonic wavenumber [47].

3.5.4. The global reactivity parameters

The highest occupied molecular orbital's (HOMO) and the lowest unoccupied molecular orbital's (LUMO) were displayed in Fig. S11 (Supplementary Materials). Interestingly, upon the ion –ligand interactions, the HOMOs of the metallic complexes were located on the side of Q1a and Q2a, while the LUMOs were situated on Q1b and Q2b, respectively. In addition, the presence of water molecules in the inner sphere plays a crucial role in the stabilization of the complexes.

The frontier molecular orbitals (HOMO and LUMO) are at the heart of chemical reactivity. The gaps $\Delta E = HOMO - LUMO$ of the copper (spinα = 6.759 eV, spinβ = 6.800 eV) and zinc complexes (6.745 eV) were lower than that of their corresponding ligands Q1 (7.165 eV), and Q2 (7.132 eV). These findings supported the obtained complexes that are relatively more reactive and therefore more bioactive than the corresponding free ligands.

Using the Koopman's theorem for closed-shell molecules [48], the HOMO and LUMO were used to predict global reactivity parameters, such as the chemical potential ($\mu = (I + A)/2$), the hardness ($\eta = (I - A)/2$), the electrophilicity index ($\omega = \mu^2/2\eta$), the softness ($S = 1/2\eta$). These parameters are used to recognize the connection concerning structure, stability and global chemical reactivity of molecules. The obtained results are summarized in Table 2.

The hardness η, the softness S and the electrophilicity indexes ω values indicate that the complexes are less hard, more soft, and more polarizable then the free ligands, making HQ1 and HQ2 act as nucleophiles while metallic ions as electrophiles. In addition, according to Sanderson's principle [49,50], the comparison of the chemical potentials values of the reactants to their corresponding complexes, as displayed in equations (1) and (2) :

$$\mu_{Cu^{2+}} \langle \mu_{copper \quad complex} \langle \mu_{HQ1} \quad (1)$$

$$\mu_{Zn^{2+}} \langle \mu_{zinc \ \ complex} \langle \mu_{HQ2} \quad (2)$$

indicated that during the evolution of the complexation reaction, a flow of electronic density takes place from the donor (HQ1 or HQ2) to the acceptor (copper or zinc ions) in order to balance the electron chemical potential of the new system.

3.5.5. Natural Atomic Orbital (NAO) and Natural Bond orbital (NBO) analysis

Tables 3, 4 present the Natural Electron Configuration (NEC) of the copper(II), zinc(II) and the oxygen atoms in their vicinity. As shown in Fig. 2, it was important to keep in mind that the implied oxygen atoms are those of the carboxylic groups (O10, O28), those of the carbonyl group (O2 and O33) and that of the water molecule in the inner sphere (O54). For the zinc complex (Fig. S9 in Supplementary Materials), the corresponding oxygen atoms are O2, O34, O7,O39 and O21, in the same sequence.

The electronic arrangement of the Cu and Zn ions in the investigated complexes were $[Ar]4s^{0.33}3d^{9.11}4p^{0.41}5p^{0.01}$ and $[Ar]4s^{0.33}3d^{9.94}4p^{0.44}5p^{0.01}$, respectively. The occupancies of d orbitals are in the same order $d_{xy}^{1.98704}d_{xz}^{1.97717}d_{yz}^{1.8583}d_{x^2-y^2}^{1.32876}d_{z^2}^{1.95697}$ and $d_{xy}^{1.99151}d_{xz}^{1.99301}d_{yz}^{1.98351}d_{x^2-y^2}^{1.98983}d_{z^2}^{1.98484}$. The differences between the d-orbital occupancies of the ions ($3d^{9.11}$ and $3d^{9.94}$) after complexation (Table 3) and that in the free ion ($3d^9$ and $3d^{10}$) were negligible.

The electronic arrangement of the Cu and Zn ions in the investigated complexes was $[Ar]\ 4s^{0.33}3d^{9.11}4p^{0.41}5p^{0.01}$ and $[Ar]\ 4s^{0.33}3d^{9.94}4p^{0.44}5p^{0.01}$, respectively. The occupancies of d orbitals in the same order are $d_{xy}^{1.98704}d_{xz}^{1.97717}d_{yz}^{1.8583}d_{x^2-y^2}^{1.32876}d_{z^2}^{1.95697}$ and $d_{xy}^{1.99151}d_{xz}^{1.99301}d_{yz}^{1.98351}d_{x^2-y^2}^{1.98983}d_{z^2}^{1.98484}$ and the differences between the d-orbital occupancies of the ions ($3d^{9.11}$ and $3d^{9.94}$) after complexation and that in the free ion ($3d^9$ and $3d^{10}$) were negligible.

In addition, the natural charges on the Cu (II) and Zn (II) ions (+2.0e) changed significantly after complexation (0.846e and 0.913e), showing that electron transfer occurred from O (2s, 2p) orbitals to Cu(II) or Zn(II) orbitals (4s, 4p). The most affected oxygen atoms were O2 and 033 in the first complex and O7 and O39 in the second one.

For deeper insight into the nature and strength of the bonds between metallic (II) ions and neighboring oxygen atoms, the Wiberg bond indexes (WBIs) [31–53] were estimated. The relative findings reported in Table 4 and Table S5 (Supplementary Materials) show that the covalent character of these bonds was weak. The highest

Table 2
Global reactivity parameters values (in eV) of HQ1, HQ2, copper and zinc complexes.

	HQ1	Cu(II) Spin α	Spin β	Complex Spin α	Spin β	HQ2	Zn(II)	Complex
E_{LUMO}	0.082	-2.400	-2.411	-0.506	-0.512	0.114	-3.350	-0.351
E_{HOMO}	-7.083	-5.815	-5.821	-7.265	-7.312	-7.018	-5.946	-7.096
A	-0.082	2.400	2.411	0.506	0.512	-0.114	3.350	0.351
I	7.083	5.815	5.821	7.265	7.312	7.018	5.946	7.096
ΔE	7.165	3.415	3.410	6.759	6.800	7.132	2.596	6.745
η	3.582	1.708	1.705	3.380	3.400	3.566	1.296	3.372
μ	-3.501	-4.108	-4.116	-3.886	-3.912	-3.452	-4.648	-3.723
ω	1.711	4.940	4.968	2.234	2.250	1.670	8.321	2.055
S	0.279	0.586	0.587	0.296	0.294	0.281	0.770	0.297

Table 3
The natural atomic charges, total natural populations (TNPs) and natural electron configurations of selected atoms in Cu(II) and Zn(II) complexes as calculated at the CAM-B3LYPD3BJ /6-31g(d) level of theory.

Atom	TNP	Natural Electron Configuration
Cu	27.86	[core]$4s^{0.33}3d^{9.11}4p^{0.41}5p^{0.01}$
O10	8.8	[core]$2s^{1.67}2p^{5.12}3p^{0.01}$
O28	8.77	[core]$2s^{1.67}2p^{5.08}3p^{0.01}3d^{0.01}$
O2	8.66	[core]$2s^{1.65}2p^{4.99}3p^{0.01}3d^{0.01}$
O33	8.68	[core]$2s^{1.66}2p^{5.00}3p^{0.01}3d^{0.01}$
O54	8.98	[core]$2s^{1.72}2p^{5.24}3p^{0.01}3d^{0.01}$
Zn	28.72	[core]$4s^{0.33}3d^{9.94}4p^{0.44}5p^{0.01}$
O2	8.82	[core]$2s^{1.67}2p^{5.14}3p^{0.01}$
O34	8.83	[core]$2s^{1.68}2p^{5.14}3p^{0.01}$
O7	8.72	[core]$2s^{1.66}2p^{5.05}3p^{0.01}$
O39	8.70	[core]$2s^{1.65}2p^{5.03}3p^{0.01}3d^{0.01}$
O21	9.00	[core]$2s^{1.71}2p^{5.27}3p^{0.01}3d^{0.01}$

Table 4
Natural Atomic Orbital (NAO) of Cu (II) and neighboring oxygen atoms.

Contribution	Center 1	NAO	Center 2	NAO	Total WBI
0.0675	Cu1	4s		2p	
0.0649		4p	O10	2s	0.3463
0.0811		4p		2p	
0.0779		3d		2p	
0.0743	Cu1	4s		2p	
0.0720		4p	O28	2s	0.4115
0.0907		4p		2p	
0.1110		3d		2p	
0.0721		4s		2p	
0.0628	Cu1	4p	O2	2s	0.3146
0.0757		4p		2p	
0.0540		3d		2p	
0.6320	Cu1	4s		2p	
0.0588		4p	O33	2s	0.2704
0.0656		4p		2p	
0.0658	Cu1	4s	O54	2p	0.1871

values of WBI 0.4115, 0.3463 0.3151 and 0.2825 were assigned to Cu1-O28, Cu1-O10, Zn1-O2, and Zn1-O34 bonds, respectively.

Interestingly, as shown in Eq.3-5 the shorter the inter-atomic bond, the higher the value of WBI:

$$WBI_{Cu\text{-}O28\ (1.286\ Å)} > WBI_{Cu\text{-}O10\ (1.902\ Å)} > WBI_{Cu\text{-}O2\ (1.946\ Å)} > WBI_{Cu\text{-}O33\ (2.000\ Å)} > WBI_{Cu\text{-}O54(2.200\ Å)} \quad (3)$$

$$WBI_{Zn\text{-}O2\ (1.909\ Å)} > WBI_{Zn\text{-}O34\ (1.948\ Å)} > WBI_{Zn\text{-}O21\ (2.021\ Å)} > WBI_{Zn\text{-}O39\ (2.026\ Å)} > WBI \quad (4)$$

The water molecule was attracted more strongly by Zn(II) than by Cu (II):

$$WBI_{Zn\text{-}O21\ (2.021\ Å)} > WBI_{Cu\text{-}O54\ (2.200\ Å)} \quad (5)$$

Additionally, the identification of the orbitals responsible for the interactions between the metallic ions and the oxygen was carried out by the decomposition of WBI in NAO basis from which it was revealed that, for the Cu1-O28, Cu1-O10 and Cu1-O2 bonds, the dominant interactions were 3d(Cu)- 2p(O) and 4p(Cu)- 2p(O). However in the zinc complex only 4p-2p and 4p-2s interactions were observed.

The NBO analysis [54], also performed at the CAM-B3LYPD3BJ /6-31g(d) level of theory, provided details about the most important migrations and their corresponding second-order interaction energies E(2) which indicates the intensity of the interaction between the electron donor and acceptor orbitals. The greater value of E(2), the more tendency of a higher donor orbital. The BD, LP, BD* denoted the occupied bonding orbitals, the lone pairs and the empty antibonding orbitals, respectively.

The strongest interactions playing a crucial role in the stabilization of the copper and zinc complexes were reported respectively in Table 5 and Table S6 (Supplementary Materials). For the first complex, following comments could be mainly highlighted:

- ü Migrations from the lone pairs (LP*) of O10 and O28 to the BD* Cu(II) orbitals. The most important ones had high energies of 21.33, 24.44, 19.95 and 34.73 kcal/mol.
- ü Interactions between the carbonyl oxygen orbitals of O2 and O33, and the metallic ion : LP(2)O2 →LP*(6)Cu1 (E=34.73 kcal/mol.) and LP(2)O33→ BD*(1)Cu1-O2 (19.95 kcal/mol.).
- ü The BD*(1) Cu1-O2 → LP*(1)C3 and BD*(1)Cu1-O2 → LP*(1)C32 migrations starting from Cu-O2 or Cu-O33 to the carbons (C3 or C32) of the carbonyl groups. The corresponding energies were of the order of E=102 kcal/mol. They were represented in a sense, solid bridges between the two molecules of the Q2 ligand.
- ü Migrations involving water molecules and the metal ion, or donor atoms constituting the ligand such as O10, N43 or F53. The most energetic ones were LP(2) O54 → BD*(1)Cu1-O33(E=16.02 kcal/mol.), LP(1)O10 → π*(1)O58-H110 (E=9.91 kcal/mol.)
- ü Finally, the interactions involving hydrogen bonding between the complex and water molecules also played a role in the stabilization of the complex: LP(2)O58 → π*(1)O54-H105 (E=17.20 kcal/mol.), LP(2)O57 → π*(1)O55-H104(E= 14.78 kcal/mol.) and LP(2)O56 → π*(1)O59-H113 (E= 12.83kcal/mol.).

The zinc complex was stabilized by almost the same type of migrations. The most energetic ones were LP(2)O2 → LP*(6)Zn1(E= 50.49 kcal/mol.), LP(2)O34 → LP*(6)Zn1 (E= 42.81kcal/mol.), LP(2)O39→ LP*(6)Zn1(E=37.55 kcal/mol.) and LP(2)O69 → BD*1)O21-H32 (E= 48.76 kcal/mol.).

3.5.6. QTAIM analysis

The different intermolecular interactions stabilizing the studied metal complexes were explored with the topological analysis of the

Table 5
Second- order interaction energy ($E^{(2)}$, in kcal/mol.) between the donor and acceptor orbitals in the copper (II) complex calculated at CAM-B3LYPD3BJ /6-31g(d) level of theory.

Complex	Donor → Acceptor		$E^{(2)}$ kcal/mol.
$[Cu(Q1)_2H_2O].6H_2O$	LP(2)O10	→ LP*(7)Cu1	21.33
	LP(1)O10	→ LP*(7)Cu1	3.84
	LP(2)O28	→ LP*(6)Cu1	24.44
	LP(1)O28	→ LP*(6)Cu1	5.71
	LP(2)O2	→ LP*(6)Cu1	34.73
	LP(2)O33	→ BD*(1)Cu1-O2	19.95
	LP(2)O10	→ BD*(1)Cu1-O2	4.47
	LP(2)O10	→ BD*(1)Cu1-O33	9.28
	LP(1)O10	→ BD*(1)Cu1-O33	3.68
	LP*(6)Cu1	→ BD*(1)Cu1-O2	10.22
	LP*(5)Cu1	→ BD*(1)Cu1-O33	6.61
	BD*(1)Cu1-O2	→ LP*(1)C3	102.02
	BD*(1)Cu1-O33	→ LP*(1)C32	102.02
	LP(2)O54	→ LP*(6)Cu1	5.02
	LP(2)O54	→ BD*(1)Cu1-O33	16.02
	π(1)O54-H105	→ π*(1)Cu1-O33	2.50
	π(1)O54-H108	→ π*(1)Cu1-O33	1.05
	LP (1) N43	→ π* (1) O56 -H	6.61
	LP(1)F53	→ π*(1)O57-H107	1.00
	LP(1)O10	→ π*(1)O58-H110	9.91
	LP(2)O58	→ π*(1)O54-H105	17.20
	LP(1)O55	→ π* (1)C48-H96	1.23
	LP(2)O55	→ π*(1)O60-H115	9.80
	LP(2)O56	→ π*(1)O59-H113	12.83
	LP(2)O57	→ π*(1)O55-H104	14.78
	LP(2)O59	→ π*(1)O60-H116	10.92
	LP(2)O60	→ π*(1)O56-H112	8.23
	LP(1)O60	→ π*(1)O57-H106	4.96
	LP(2)O60	→ π*(1)O56-H112	8.23

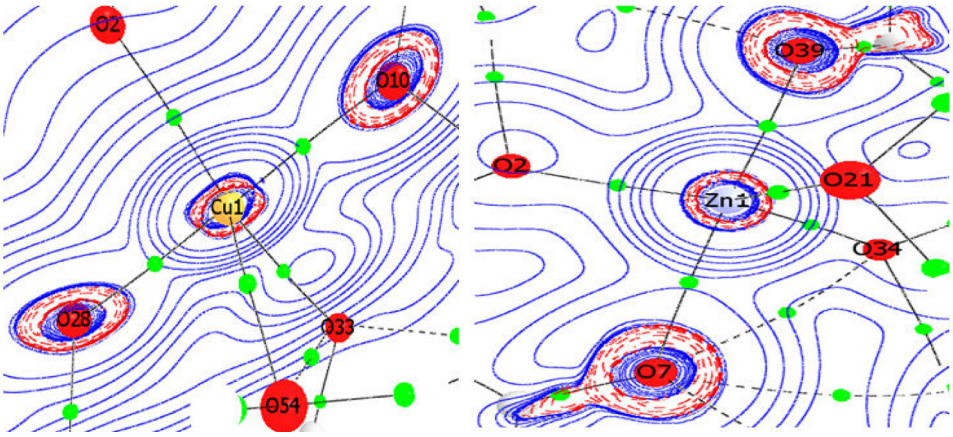

Fig. 11. Maps of the Laplacian of the electron density in the complexes through the O10- Cu1-O28 and O7-Zn-O39 planes.

electron, within the conceptual framework of the quantum theory of atoms in molecules (QTAIM) [55–62].

Among the topological properties of the electron density that were successfully used to analyze the bonding in the complexes, the electron density at the bond critical point ρ(r), the Laplacian of the electron density $\nabla^2\rho$(r), the potential electron energy density($V_{(r)}$), the local gradient kinetic energy density ($G_{(r)}$) and the total electron energy density ($H_{(r)}$) [63–65], were of fundamental importance.

QTAIM analysis allowed the localization of interactions that contribute to the stabilization of the complexes. Important BCPs were observed between the metal ion and neighboring oxygen atoms (Fig. 11), between ligand and water molecules, and between two neighboring water molecules. The corresponding BCPs topological data are reported in Table 6.

To investigate the nature and the strength of these interactions, $\nabla^2\rho_{(r)}$ and $H_{(r)}$ were used as descriptors. For all bonds, the values of ρ(r) were small ($\simeq 10^{-2}$ a.u) and those of $\nabla^2\rho(r) > 0$ ranging from +0.24483 a.u to +0.8388 a.u for the copper complex and from 0.3570 a.u to 0.5890 a.u, for the zinc complex. These findings characterize the closed-shell interactions [66,67] which were mostly dative when $H_{(r)} < 0$ and weakly ionic when $H_{(r)} > 0$ (Cu1-O28, Cu1-O10). Additionally, for the cases where $0.5 < -\frac{G_{(r)}}{V_{(r)}} < 1$, covalent character is dominant [68].

The other interactions Q1-H_2O, Q2-H_2O and H_2O - H_2O were of the hydrogen bonding type [69,70]. From their classification, the interactions were medium when $\nabla^2\rho_{(r)} > 0$ and $H_{(r)} > 0$ or weak when $\nabla^2\rho_{(r)} > 0$ and $H_{(r)} < 0$.

3.5.7. Visualization of non-covalent interactions in the complexes

Among the quantum mechanical methods, the reduced density gradient analysis has been of an ongoing interest in the detection and the visualization of non-covalent interactions (NCI) [71–74].

Table 6
Selected topological parameters of ρ(r) function for intramolecular bondings in Cu(II) and Zn(II) complexes.

	BCP	ρ(r)	$\nabla^2\rho$(r)	$V_{(r)}$	$G_{(r)}$	$H_{(r)}$	$\lvert V_{(r)}\rvert/G_{(r)}$	$-G_{(r)}/V_{(r)}$
	Cu(II)···Q1, Cu(II)··· H_2O							
[Cu(Q1)$_2$ H_2O].6H_2O	O28···Cu1	0.0703	0.8388	-0.2028	0.2062	0.0034	0.9835	1.0168
	Cu1···O10	0.0624	0.7004	-0.1736	0.1743	0.0007	0.9960	1.0040
	O33···Cu1	0.0570	0.4195	-0.1318	0.1184	-0.0134	1.1132	0.8983
	Cu1···O2	0.0615	0.5475	-0.1565	0.1467	-0.0098	1.0668	0.9374
	Cu1…O54	0.0361	0.2483	-0.0719	0.067	-0.0049	1.0731	0.9318
	Q1···H_2O							
	O33···O54	0.0073	0.0406	-0.0107	0.0104	-0.0003	1.0288	0.1720
	H96···O55	0.0110	0.0446	-0.0099	0.0106	0.0007	0.9340	1.0707
	N43···H111	0.0249	0.1132	-0.0303	0.0293	-0.001	1.0341	0.9670
	O56···F53	0.0061	0.0360	-0.0065	0.0077	0.0012	0.8442	1.1846
	F53···H107	0.0128	0.0707	-0.0162	0.0169	0.0007	0.9586	1.0432
	H104···O57	0.0318	0.1905	-0.0489	0.0483	-0.0006	1.0124	0.9877
	H110···O10	0.0304	0.1731	-0.0436	0.0435	-0.0001	1.0023	0.9977
	O33···O58	0.0058	0.0294	-0.0055	0.0064	0.0009	0.8594	1.1636
	H94···O59	0.0046	0.0204	-0.0032	0.0041	0.0009	0.7805	1.2813
	H94···O56	0.0051	0.0234	-0.0035	0.0047	0.0012	0.7447	1.3429
	H98···H109	0.0038	0.0199	-0.0024	0.0037	0.0013	0.6486	1.5417
	H94···O60	0.0050	0.0221	-0.0033	0.0044	0.0011	0.7500	1.3333
	H_2O ···H_2O							
	H105···O58	0.0346	0.2187	-0.0562	0.0554	-0.0008	1.0144	0.9858
	H113···O56	0.0299	0.1732	-0.0443	0.0438	-0.0005	1.0114	0.9887
	O55···H115	0.0269	0.1461	-0.0377	0.0372	-0.0005	1.0134	0.9867
	O59···H116	0.0279	0.1561	-0.04	0.0395	-0.0005	1.0127	0.9875
	H112···O60	0.0261	0.1353	-0.0356	0.0347	-0.0009	1.0259	0.9747
	O60···H106	0.0244	0.1322	-0.0326	0.0328	0.0002	0.9939	1.0061
[Zn(Q2)$_2$ H_2O].3H_2O	Zn(II) ···Q2, Zn(II) ···H_2O							
	O2···Zn1	0.0720	0.5890	-0.1867	0.1669	-0.0198	1.1186	0.8939
	Zn1··· O34	0.0658	0.5113	-0.1649	0.1464	-0.0185	1.1264	0.8878
	Zn1···O7	0.0473	0.3570	-0.1066	0.0979	-0.0087	1.0889	0.9184
	O39···Zn1	0.0533	0.3985	-0.1241	0.1119	-0.0122	1.1090	0.9017
	O21…Zn1	0.0543	0.4091	-0.1294	0.1158	-0.0136	1.1174	0.8949
	$Q2_a$···$Q2_b$, Q2···H_2O							
	H67···O2	0.0264	0.1443	-0.0368	0.0365	-0.0003	1.0082	0.9918
	O34···O7	0.0076	0.0481	-0.0108	0.0114	0.0006	0.9474	1.0556
	H70···O7	0.0164	0.0753	-0.0184	0.0186	0.0024	0.9871	1.0131
	O63···H31	0.0086	0.0337	-0.0075	0.0079	0.0004	0.9494	1.0533
	O7···O63	0.0054	0.0301	-0.0054	0.0065	0.0011	0.8308	1.2037
	O34···H65	0.0302	0.1700	-0.0432	0.0429	-0.0003	1.0070	0.9931
	O66···O39	0.0051	0.0268	-0.0049	0.0058	0.0009	0.8448	1.1837
	H62···O66	0.0160	0.0690	-0.0174	0.0173	-0.0001	1.0058	0.9943
	O36···H64	0.0137	0.0632	-0.0149	0.0154	0.0005	0.9675	1.0336
	H32···O69	0.0398	0.2832	-0.0737	0.0723	-0.0014	1.0194	0.9810
	H_2O···H_2O							
	H71···O63	0.0320	0.1984	-0.0503	0.0500	-0.0003	1.0060	

This approach, which is equivalent to the Lewis model in bonding, utilizes the reduced density gradient s(r) or RDG(r) as an analysis index [75]:

$$s(r)\ or\ RDG(r) = \frac{1}{2(3\pi^2)^{1/3}} \frac{|\nabla\rho(r)|}{\rho(r)^{4/3}} \sqrt{a^2 + b^2} \qquad (6)$$

The interaction type that developed in the studied zinc complex (Fig. 12) was distinguished as isosurfaces in the 2D representation where the RDG (r) was plotted against sign (λ) multiplied by electron density as the ordinate.

The attractive bonds (ρ >0, λ_2<0) including dative and hydrogen bonds were energetically located at -0.45 a.u, -0.03 a.u and -0.02 a.u. The region of vdW forces is depicted by the two spikes in the middle of the scatter map. However, the region of the strong steric effects (ρ >0, λ_2>0) was characterized by two peaks between 0.01 and 0.02 a.u.

In the 3D representation (Fig. 13) plotted by the VMD program [76], the revealing of different types of the interactions achieved using colors: blue, green and red colors indicating attractive bonds, van der Waals and repulsive interactions, respectively. As illustrated in this figure, for the zinc complex the color corresponding to attractive bonds was observed between (Zn1, O39), (Zn1, O21), (H32, O69), (H71, O63), (H65, O34) and (H67, O2). Van der Waals interactions were located between (H64, O36), (H31, O63), (H65, O7), (H62, O66) and (H32, O7). However, the steric effects that influence the stability of the complex were observed within the segments O34-C35-C37-C38-O39 and O2-C3-C5-C6-O7. One can easily notice that RDG findings were in good agreement with QTAIM and NBO results. For the copper complex, the results are shown in Fig. S12 (Supplementary Materials).

4. Conclusion

Two solid-state complexes of copper(II) and zinc (II) with enrofloxacin and oxolinic acid have been synthesized and characterized using single–crystal X-ray diffraction, Hirshfeld surface and ^{1}H NMR spectroscopy. Interestingly, the structure of the complexes does not include co-ligands in the internal coordination sphere.

In our study, we used HS analysis to determine the crystal structure packing of two complexes. We found that the small spots in the HS plots were associated with C-H···π interactions, while the shape index revealed weak π···π stacking interactions in both complexes. Additionally, the fingerprint plots indicated that H···H and H···O/O···H interactions were the most prevalent in the crystal structures of the Cu(II) and Zn(II) complexes.

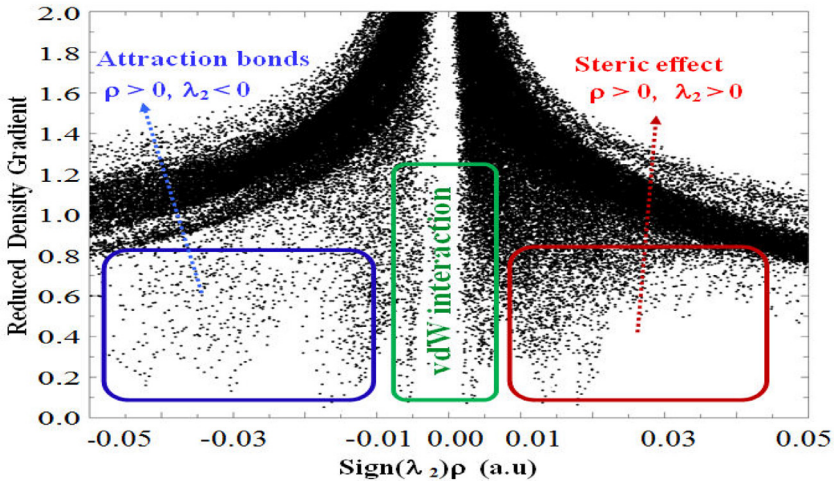

Fig. 12. 2D RDG NCI isosurface for zinc (II) complex computed at the CAM-B3LYP/6-31g(d) level of theory.

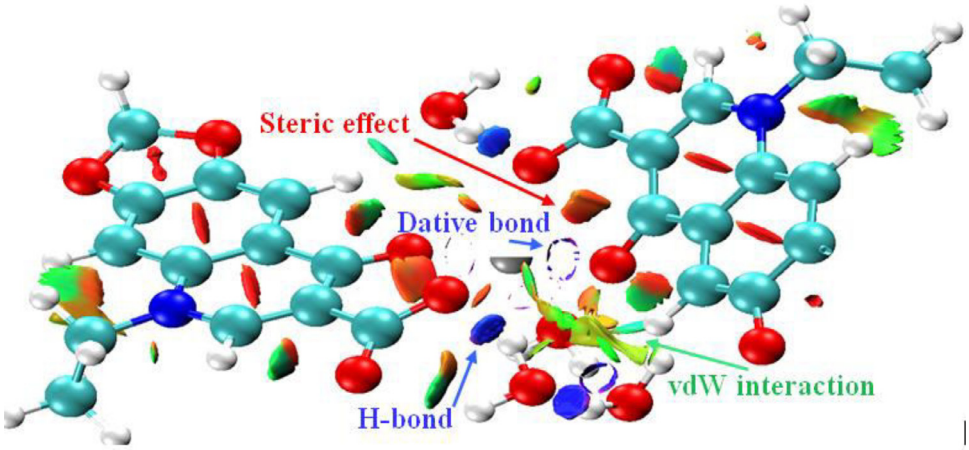

Fig. 13. 3D RDG representation of NCI for Zn(II) complex.

In the modeling part, the CAM-B3LYPD3BJ exchange functional including the dispersion correction performs better than CAM-B3LYP in predicting structural parameters and vibration frequencies of the molecule complex.

Upon the complexation formation, the properties of $[Cu(Q1)_2H_2O].6H_2O$ and $[Zn(Q2)_2H_2O].4H_2O$ are different from those of the free reactants (Q1 and Q2). Many significant modifications were reported in length bonds, Mulliken charges and in potential electrostatic values.

Important information on the Cu (II) and Zn (II) complexes structures and properties were obtained upon NAO and NBO calculations. Then, non covalent interactions in the formed complexes were explored and visualized through QTAIM and RDG topologic tools.

CRediT statement

Amina Boughougal: Writing-original draft, investigation, DFT, software, synthesis, docking. **Rayene Kadri:** Spectroscopic studies, DFT, software. **Mekki Kadri:** DFT study, Supervision, Writing - review & editing. **Jean Bernard Tommasino:** crystallographic study. **Guillaume Pilet:** Synthesis and characterization of the copper and zinc complexes . **Amel Messai:** Spectrscopic and crystallographic study studies . **Dominique Luneau:** Synthesis and characterization of the copper and zinc complexes

Declaration of Competing Interest

The authors declare that they have no known competing financial interests or personal relationships that could have appeared to influence the work reported in this paper.

Data Availability

No data was used for the research described in the article.

Acknowledgments

We extend our gratitude to the Algerian Minister of Higher Education and Scientific Research and the ATRST for their support through the P.R.F.U project. We would also like to express our sincere appreciation to Noureddine Dadda and Abdenour Guerraoui for their assistance in conducting the Hirshfield surface calculations and to Meryem Goudjil for her valuable contributions.

Supplementary materials

Supplementary material associated with this article can be found, in the online version, at doi:10.1016/j.molstruc.2023.135141.

References

[1] T. Takeuchi, A. Böttcher, C.M. Quezada, T.J. Meade, H.B. Gray, Inhibition of thermolysin and human α-thrombin by cobalt (III) Schiff base complexes, J. Bioorg. Med. Chem. 7 (1999) 815–819, doi:10.1016/S0968-0896(98)00272-7.

[2] A. Boughougal, F.Z. Cherchali, A. Messai, N. Attik, D. Decoret, M. Hologne, S. Corinne, P. Guillaume, J.B. Tommasino, D. Luneau, New model of metallo antibiotic: synthesis, structure and biological activity of a zinc(II) mononuclear complex carrying two enrofloxacin and sulfadiazine antibiotics, J. New. J. Chem. 42 (18) (2018) 15346–15352, doi:10.1016/S0968-0896(98)00272-7org/10.1039/C8NJ01774C.

[3] G. Psomas, D.P. Kessissiglou, Quinolones and non-steroidal anti-inflammatory drugs interacting with copper (II), nickel (II), cobalt (II) and zinc (II): structural features, biological evaluation and perspectives, J. Chem. Soc., Dalton Trans. 42 (18) (2013) 6252–6276, doi:10.1039/C3DT50268F.

[4] F.M. Aarestrup, A.M. Seyfarth, H.D. Emborg, K. Pedersen, R.S. Hendriksen, F. Bager, Effect of abolishment of the use of antimicrobial agents for growth promotion on occurrence of antimicrobial resistance in fecal enterococci from food animals in Denmark, Antimicrob. Agents Chemother 47 (2001) 2054–2059, doi:10.1128/AAC.45.7.2054-2059.2001.

[5] A. Mustaev, M. Malik, X. Zhao, N. Kurepina, G. Luan, M.L. Oppegard, H. Hiroshi, R.M. Kevin, J.K. Robert, M.B. James, K. Drlica, Fluoroquinolone-gyrase-DNA complexes: two modes of drug binding, J. Biol. Chem. 289 (18) (2014) 12300–12312, doi:10.1074/jbc.M113.529164.

[6] J.M. Recillas, A.M. Flores, E.R. Moreno, M.J. Gracia, A copper (II) complex of 1, 10-phenanthroline and enrofloxacin, J. Acta Crystallogr. E: Crystallogr. 63 (12) (2007) m3030–m3031, doi:10.1107/S1600536807057649.

[7] E.K. Efthimiadou, A. Karaliota, G. Psomas, Mononuclear dioxomolybdenum (VI) complexes with thequinolones enrofloxacin and sparfloxacin: synthesis, structure, antibacterial activity and interaction with DNA, J. Polyhedron. 27 (1) (2008) 349–356, doi:10.1016/j.poly.2007.09.013.

[8] E.K. Efthimiadou, A. Karaliota, G. Psomas, Mononuclear metal complexes of the second-generation quinolone antibacterial agent enrofloxacin: synthesis, structure, antibacterial activity and interaction with DNA, J. Polyhedron 27 (6) (2008) 1729–1738, doi:10.1016/j.poly.2008.02.006.

[9] E.K. Efthimiadou, Y. Sanakis, M. Katsarou, C.P. Raptopoulou, A. Karaliota, N. Katsaros, G. Psomas, Neutral and cationic mononuclear copper (II) complexes with enrofloxacin: structure and biological activity, J. Inorg. Biochem. 100 (8) (2006) 1378–1388, doi:10.1016/j.jinorgbio.2006.03.013.

[10] K.C. Skyrianou, V. Psycharis, C.P. Raptopoulou, D.P. Kessissoglou, G. Psomas, Nickel–quinolones interaction. Part 4—Structure and biological evaluation of nickel (II)–enrofloxacin complexes compared to zinc (II) analogues, J. Inorg. Biochem. 105 (1) (2011) 63–74, doi:10.1016/j.jinorgbio.2010.09.007.

[11] N.E.A. El-Gamel, Silver (I) complexes as precursors to produce silver nanowires: structure characterization, antimicrobial activity and cell viability, J. Chem. Soc., Dalton Trans. 27 (2013) 9884–9892, doi:10.1039/C3DT33092C.

[12] Y.J. Wang, R.D. Hu, D.H. Jiang, P.H. Zhang, Q.Y. Lin, Y.Y. Wang, Synthesis, crystal structure, interaction with BSA and antibacterial activity of La (III) and Sm (III) complexes with enrofloxacin, J. Fluoresc. 21 (2011) 813–823, doi:10.1007/s10895-010-0775-1.

[13] M. Zampakou, M. Akrivou, E.G. Andreadou, C.P. Raptopoulou, V. Psycharis, A.A. Pantazaki, G. Psomas, Structure, antimicrobial activity, DNA-and albumin-binding of manganese (II) complexes with the quinolone antimicrobial agents oxolinic acid and enrofloxacin, J. Inorg. Biochem. 121 (2013) 88–99, doi:10.1016/j.jinorgbio.2012.12.013.

[14] K.C. Skyrianou, F. Perdih, I. Turel, D.P. Kessissoglou, G. Psomas, Nickel–quinolones interaction. Part2–Interaction of nickel (II) with the antibacterial drug oxolinic acid, J. Inorg. Biochem. 104 (2) (2010) 161–170, doi:10.1016/j.jinorgbio.2009.10.017.

[15] A. Tarushi, P. Christofis, G. Psomas, Synthesis, characterization and interaction with DNA of mononuclear metal complexes with oxolinic acid, J. Polyhedron. 26 (14) (2007) 3963–3972, doi:10.1016/j.poly.2007.04.031.

[16] K.C. Skyrianou, F. Perdih, A.N. Papadopoulos, I. Turel, D.P. Kessissoglou, G. Psomas, Nickel–quinolones interaction: part 5-biological evaluation of nickel (II) complexes with first-, second-and third-generation Quinolones, J. Inorg. Biochem. 105 (10) (2011) 1273–1285, doi:10.1016/j.jinorgbio.2011.06.005.

[17] A. Tarushi, K. Lafazanis, J. Kljun, I. Turel, A.A. Pantazaki, G. Psomas, D.P. Kessissoglou, First-and second-generation quinolone antibacterial drugs interacting with zinc (II): structure and biological perspectives, J. Inorg. Biochem. 121 (2013) 53–65, doi:10.1016/j.jinorgbio.2012.12.009.

[18] A. Tarushi, G. Psomas, C.P. Raptopoulou, D.P. Kessissoglou, Zinc complexes of the antibacterial drug oxolinic acid: structure and DNA-binding properties, J. Inorg. Biochem. 103 (6) (2009) 898–905, doi:10.1016/j.jinorgbio.2009.03.007.

[19] H. Kargar, M. Ashfaq, M. Fallah-Mehrjardi, R. Behjatmanesh-Ardakani, K.S. Munawar, M.N. Tahir, Theoretical studies, Hirshfeld surface analysis, and crystal structure determination of a newly synthesized benzothiazole copper (II) complex, J. Mol. Struct 1261 (2022) 132905, doi:10.1016/j.molstruc.2022.132905.

[20] H. Kargar, M. Fallah-Mehrjardi, R. Behjatmanesh-Ardakani, H.A. Rudbari, A.A. Ardakani, S. Sedighi-Khavidak, M.N. Tahir, Binuclear Zn (II) Schiff base complexes: synthesis, spectral characterization, theoretical studies and antimicrobial investigations, J. Inorganica Chim. Acta 530 (2022) 120677, doi:10.1016/j.ica.2021.120677.

[21] H. Kargar, A.A. Ardakani, M.N. Tahir, M. Ashfaq, K.S. Munawar, Synthesis, spectral characterization, crystal structure and antibacterial activity of nickel (II), copper (II) and zinc (II) complexes containing ONNO donor Schiff base ligands, J. Mol. Struct. 1233 (2021) 130112, doi:10.1016/j.molstruc.2021.130112.

[22] H. Kargar, F. Aghaei-Meybodi, M.R. Elahifard, M.N. Tahir, M. Ashfaq, K.S. Munawar, Some new Cu (II) complexes containing O, N-donor Schiff base ligands derived from 4-aminoantipyrine: synthesis, characterization, crystal structure and substitution effect on antimicrobial activity, J. coord Chem. 74 (9–10) (2021) 1534–1549, doi:10.1080/00958972.2021.1900831.

[23] H. Kargar, F. Aghaei-Meybodi, R. Behjatmanesh-Ardakani, M.R. Elahifard, V. Torabi, M. Fallah-Mehrjardi, K.S. Munawar, Synthesis, crystal structure, theoretical calculation, spectroscopic and antibacterial activity studies of copper (II) complexes bearing bidentate Schiff base ligands derived from4-amino antipyrine :influence of substitutionson antibacterial activity, J. Mol. Struct. 1230 (2021) 129908, doi:10.1016/j.molstruc.2021.129908.

[24] A. Tarushi, G. Psomas, C.P. Raptopoulou, V. Psycharis, D.P. Kessissoglou, Structure and DNA-binding properties of bis (quinolonato) bis (pyridine) zinc (II) complexes, J. Polyhedron. 28 (15) (2009) 3272–3278, doi:10.1016/j.poly.2009.04.003.

[25] G. Psomas, A. Tarushi, E.K. Efthimiadou, Y. Sanakis, C.P. Raptopoulou, N. Katsaros, Synthesis, structure and biological activity of copper (II) complexes with oxolinic acid, J. Inorg. Biochem. 100 (11) (2006) 1764–1773, doi:10.1016/j.jinorgbio.2006.06.012.

[26] T. Yanai, D.P. Tew, N.C. Handy, A new hybrid exchange–correlation functional uses the Coulomb-attenuating method (CAM-B3LYP), J. Chem. Phys. Lett. 393 (1–3) (2004) 51–57, doi:10.1016/j.cplett.2004.06.011.

[27] S. Grimme, S. Ehrlich, L. Goerigk, Effect of the damping function in dispersion corrected density functional theory, J. Comput. Chem. 32 (7) (2011) 1456–1465, doi:10.1002/jcc.21759.

[28] CrysAlisPro, v. 1.171.33.46 (rel. 27-08-2009 CrysAlis171.NET), Oxford Diffraction Ltd., 2009.

[29] De.J.T. Meulenaer, H. Tompa, The absorption correction in crystal structure analysis, J. Acta Crystallogr. 19 (6) (1965) 1014–1018, doi:10.1107/S0365110x65004802.

[30] R.H. Blessing, An empirical correction for absorption anisotropy, J. Acta Crystallogr, A, Found. Crystallogr. 51 (1) (1995) 33–38, doi:10.1107/S0108767394005726.

[31] M.C. Burla, R. Caliandro, M. Camalli, B. Carrozzini, G.L. Cascarano, L. De Caro, C. Giacovazzo, G. Polidori, R. Spagna, SIR 2004: an improved tool for crystal structure determination and refinement, J. Appl. Crystallogr. 36 (2003) 1103, doi:10.1107/S002188980403225X.

[32] D.J. Watkin, C.K. Prout, J.R. Carruthers, P.W. Betteridge, CRISTAL Issue 11, Vol. CRISTAL Issue 11, Chemical Crystallography Laboratory, Oxford, UK, 1999.

[33] P.R. Spackman, M.J. Turner, J.J. McKinnon, S.K. Wolff, D.J. Grimwood, D. Jayatilaka, M.A. Spackman, Crystal explorer: a program for Hirshfeld surface analysis, visualization and quantitative analysis of molecular crystals, J. Appl. Crystallogr. 54 (3) (2021) 1006–1011, doi:10.1107/S1600576721002910.

[34] J.B. Tommasino, F.N. Renaud, D. Luneau, P. Guillaume, Multi-biofunctional complexes combining antiseptic copper (II) with antibiotic sulfonamide ligands: structural, redoxand antibacterial study, J. Polyhedron. 30 (10) (2011) 1663–1670, doi:10.1016/j.poly.2011.03.033.

[35] M.J. Frisch, G.W. Trucks, H.B. Schlegel, G.E. Scuseria, M.A. Robb, J.R. Cheeseman, G. Scalmani, V. Barone, B. Mennucci, G.A. Petersson, H. Nakatsuji, M. Caricato, X. Li, H.P. Hratchian, A.F. Izmaylov, J. Bloino, G. Zheng, J.L. Sonnenberg, M. Hada, M. Ehara, K. Toyota, R. Fukuda, J. Hasegawa, M. Ishida, T. Nakajima, Y. Honda, O. Kitao, H. Nakai, T. Vreven, J.A. Montgomery, Jr., J.E. Peralta, F. Ogliaro, M. Bearpark, J.J. Heyd, E. Brothers, K.N. Kudin, V.N. Staroverov, R. Kobayashi, J. Normand, K. Raghavachari, A. Rendell, J.C. Burant, S.S. Iyengar, J. Tomasi, M. Cossi, N. Rega, J.M. Millam, M. Klene, J.E. Knox, J.B. Cross, V. Bakken, C. Adamo, J. Jaramillo, R. Gomperts, R.E. Stratmann, O. Yazyev, A.J. Austin, R. Cammi, C. Pomelli, J.W. Ochterski, R.L. Martin, K. Morokuma, V.G. Zakrzewski, G.A. Voth, P. Salvador, J.J. Dannenberg, S. Dapprich, A.D. Daniels, Ö. Farkas, J.B. Foresman, J.V. Ortiz, J. Cioslowski, and D.J. Fox, *Gaussian 09* ,Gaussian, Inc., Wallingford CT, 2009.

[36] R. Dennington, T. Keith, J. Millam, V. Gaussview, Semichem Inc, Shawnee Mission KS, 2009.

[37] J. Bernstein, R.E. Davis, L. Shimoni, N.L. Chang, Patterns in hydrogen bonding: functionality and graph set analysis in crystals, J. Angew. Chem. Int. Ed. 34 (15) (1995) 1555–1573, doi:10.1002/anie.199515551.

[38] K. Balakumaran, J. Mosesbabu, J. Anireddy, G. Chakkaravarthi, (E)-5-{4-[2-(5-Ethylpyridin-2-yl) ethoxy] benzylidene} thiazolidine-2, 4-dione, J. IUCrData 3 (1) (2018) x 171839, doi:10.1107/S2414314617018399.

[39] A. Guerraoui, A. Djedouani, E. Jeanneau, A. Boumaza, A. Alsalme, A. Zarrouk, I. Warad, Crystal structure and spectral of new hydrazine-pyran-dione derivative: DFT enol↔ hydrazone tautomerization via zwitterionic intermediate, hirshfeld analysis and optical activity studies, J. Mol Struct. 1220 (2020) 128728, doi:10.1016/j.molstruc.2020.128728.

[40] A.W. Addison, T. Rao. Ngeswara, J. Reedijk, J.V. Rijin, G.C. Verschoor, Synthesis, structure, and spectroscopic properties of copper (II) compounds containing nitrogen–sulphur donor ligands; the crystal and molecular structure of aqua [1, 7-bis (N-methylbenzimidazol-2′-yl)-2, 6-dithiaheptane] copper (II) perchlorate, J. Chem. Soc ., Dalton Trans. 7 (1984) 1349–1356, doi:10.1039/DT9840001349.

[41] H. Kargar, M. Ashfaq, M. Fallah-Mehrjardi, R. Mehdi, R. Behjatmanesh-Ardakani, K.S. Munawar, M.N. Tahir, Synthesis, crystal structure, spectral characterization, theoretical and computational studies of Ni (II), Cu (II) and Zn (II) complexes incorporating Schiff base ligand derived from 4-(diethylamino) salicylaldehyde, J. Inorganica Chim. Acta 536 (2022) 120878, doi:10.1016/j.ica.2022.120878.

[42] H. Kargar, M. Ashfaq, M. Fallah-Mehrjardi, R. Mehdi, R. Behjatmanesh-Ardakani, K.S. Munawar, M.N. Tahir, Unsymmetrical Ni (II) Schiff base complex:

synthesis, spectral characterization, crystal structure analysis, Hirshfeld surface investigation, theoretical studies, and antibacterial activity, J. Mol. Struct. 1265 (2022) 133381, doi:10.1016/j.molstruc.2021.130653.
[43] H. Kargar, M. Fallah-Mehrjardi, R. Behjatmanesh-Ardakani, K.S. Munawar, M. Ashfaq, M.N. Tahir, Titanium (IV) complex containing ONO-tridentate Schiff base ligand: synthesis, crystal structure determination, Hirshfeld surface analysis, spectral characterization, theoretical and computational studies, J. Mol. Struct. 1241 (2021) 130653, doi:10.1016/j.molstruc.2021.130653.
[44] M. Madni, M.N. Ahmed, M. Mhafeez, M. Ashfaq, M.N. Tahir, D.M. Gil, A. Frontera, Recurrent π–π stacking motifs in three new 4, 5-dihydropyrazolyl–thiazole–coumarin hybrids: X-ray characterization, Hirshfeld surface analysis and DFT calculations, J. New J. Chem. 44 (34) (2020) 14592–14603, doi:10.1039/D0NJ02931A.
[45] M.A. Spackman, J.J. Mckinnon, Fingerprinting intermolecular interactions in molecular crystals, J. CrystEngComm. 4 (66) (2002) 378–392, doi:10.1039/B203191B.
[46] A. Nataraj, V. Balachandran, T. Karthick, M. Karabacak, A. Atac, FTRaman, FT-IR, UV spectra and DFT and ab initio calculations on monomeric and dimeric structures of 3,5-pyridinedicarboxylicacid, J. Mol. Struct. 1027 (2012) 114, doi:10.1016/j.molstruc.2012.05.048.
[47] J. Spanget-Larsen, B.K.V. Hansen, P.E. Hansen, OH stretching frequencies in systems with intramolecular hydrogen bonds: harmonic and anharmonic analyses, Chem. Phys 389 (2011) 107–115, doi:10.1016/j.chemphys.2011.09.011.
[48] T. Koopmans, Ordering of wave functions and eigenenergies to the individual electrons of an atom, J. Phys. A 1 (1993) 104–113, doi:10.1016/S0031-8914(34)90011-2.
[49] R.T. Sanderson, Chemical Bonds and Bond Energy, 2nd ed., Academic Press, New York, NY, USA, 1976.
[50] K.C. Pratim, L. Hsing, G. Robert, HSAB principle, J. Am. Chem. Soc. 113 (5) (1991) 1855–1856, doi:10.1021/ja00005a073.
[51] K.B. Wiberg, Application of the pople-santry-segal CNDO method to the cyclopropylcarbinyl and cyclobutylcation and tobicyclobutane, J. Tetrahedron. 24 (3) (1968) 1083–1096, doi:10.1016/0040-4020(68)88057-3.
[52] L.K. Harper, A.L. Shoaf, C.A. Bayse, Predicting trigger bonds in explosive materials through Wiberg bond index analysis, J. Chem Phys Chem. 16 (18) (2015) 3886–3892, doi:10.1002/cphc.201500773.
[53] I. Mayer, Bond order and valence indices: a personal account, J. Comput Chem. 28 (1) (2007) 204–221, doi:10.1002/jcc.20494.
[54] A.E. Reed, L.A. Curtiuss, F. Weinhold, J. Chem. Rev. 88 (1988) 899–926.
[55] R.F.W. Bader, C.F. Matta, Bonding to titanium, J. Inorg. Chem. 40 (22) (2001) 5603–5611, doi:10.1021/ic010165o.
[56] R.F.W. Bader, H. Essén, The characterization of atomic interactions, J. Chem. Phys. 80 (5) (1984) 1943–1960, doi:10.1063/1.446956.
[57] R.F.W. Bader, Atoms in molecules, J. Acc. Chem. Re. 18 (1) (1985) 9–15, doi:10.1021/ar00109a003.
[58] R.F.W. Bader, A quantum theory of molecular structure and its applications, J. Rev. J. Chem. 91 (5) (1991) 893–928, doi:10.1021/cr00005a013.
[59] R.F.W. Bader, Atoms in Molecules: A Quantum Theory, 2nd ed., Oxford University Press, Oxford, UK, 1994.
[60] P.S.V. Kumar, V. Raghavendra, V. Subramanian, Bader's theory of atoms in molecules (AIM) and its applications to chemical bonding, J. Chem Sci. 128 (10) (2016) 1527–1536, doi:10.1007/s12039-016-1172-3.
[61] M.F. Bobrov, G.V. Popova, V.G. Tsirelson, A topological analysis of electron density and chemical bonding in cyclophosphazenes $P_nN_nX_{2n}$ (X = H, F, Cl; n = 2, 3, 4), J. Russ. J. Phys. Chem. 80 (2006) 584–590, doi:10.1134/S0036024406040182.
[62] M. Goli, S. Shahbazian, Atoms in molecules: beyond Born–Oppenheimer paradigm, J. Theor Chem. Acc. 129 (2) (2011) 235–245, doi:10.1007/s00214-011-0927-7.
[63] A.G. Nozad, S. Meftah, M.H. Ghasemi, R.A. Kiyani, M. Aghazadeh, Investigation of intermolecular hydrogen bond interactions in crystalline L-cysteine by DFT calculations of the oxygen-17, nitrogen-14, and hydrogen-2 EFG tensors and AIM analysis, J. Biophys. Chem. 141 (1) (2009) 49–58, doi:10.1016/j.bpc.2008.12.013.
[64] N.S. Venkataramanan, A. Suvitha, Nature of bonding and cooperativity in linear DMSO clusters: a DFT, AIM and NCI analysis, J. Mol. Graph. 81 (2018) 50–59, doi:10.1016/j.jmgm.2018.02.010.
[65] N.S. Venkataramanan, A. Suvitha, A. Vijayaraghavan, S. Thamotharan, Investigation of inclusion complexation of acetaminophen with pillar [5]arene: UV–Vis, NMR and quantum chemical study, J. Mol. Liq. 241 (2017) 782–791, doi:10.1016/j.molliq.2017.06.095.
[66] R. Bianchi, G. Gervasio, D. Marabello, Experimental electron density analysis of Mn2 (CO) 10: metal– metal and metal– Ligand bond characterization, J. Inorg. Chem. 39 (11) (2000) 2360–2366, doi:10.1021/ic991316e.
[67] R. Bianchi, G. Gervasio, D. Marabello, The experimental charge density in Transition metal compounds, J. C. R. Chim. 8 (2005) 1392–1399, doi:10.1016/j.crci.2004.12.015.
[68] S.A. Beyramabadi, M. Saadat-Far, A. Faraji-Shovey, M. Javan-Khoshkholgh, A. Morsali, Synthesis, experimental and computational characterizations of a new quinoline derived Schiff base and its Mn (II), Ni (II) and Cu (II) complexes, J. Mol. Struct. 1208 (2020) 127898, doi:10.1016/j.molstruc.2020.127898.
[69] F. Alexandr, L.S. Evgeniya, A.Y. Mikhali, On justification of Cu (II) environment in mononuclear complexes: Joint X-ray and AIM studies, J. Polyhedron. 30 (2011) 1710–1717, doi:10.1016/j.poly.2011.04.002.
[70] N.S. Venkataramanan, A. Suvitha, Y. Kawazoe, Intermolecular interaction in nucleo bases and dimethyl sulfoxide/water molecules: a DFT, NBO, AIM and NCI analysis, J. Mol. Graph. 78 (2017) 48–60, doi:10.1016/j.jmgm.2017.09.022.
[71] E.R. Johnson, S. Keinan, P. Mori-Sánchez, J. Contreras-García, A.J. Cohen, Y. Weitao, Revealing non covalent interactions, J. Am. Chem. Soc. 132 (18) (2010) 6498–6506, doi:10.1021/ja100936w.
[72] A. Zupan, J.P. Perdew, K. Burke, M. Causà, Density-gradient analysis for density functional theory: application to atoms, J. Int. J. Quantum Chem. 61 (5) (1997) 835–845, doi:10.1002/(SICI)1097-461X(1997)61:5<835::AID-QUA9>3.0.CO;2-X.
[73] J. Contreras-García, W. Yang, E.R. Johnson, Analysis of hydrogen-bond interaction potentials from the electron density: integration of non covalent interaction regions, J. Phys. Chem. A 115 (45) (2011) 12983–12990, doi:10.1021/jp204278k.
[74] H. Bougherara, R. Kadri, M. Kadri, M. Yekhlef, A.C. Boumaza, Complex of 4-(2-aminophenyl) – 1, 2, 3-thiadiazole with 2, 3-dichloro-5, 6-dicyano-1, 4-benzoquinone: experimental study and investigation at different exchange-correlation functionals. DOS, NBO, QTAIM and RDG analyses, J. Mol. Struct. 1223 (2021) 128855, doi:10.1016/j.molstruc.2020.128855.
[75] J.P. Perdew, M. Ernzerhof, K. Burke, Rationale for mixing exact exchange with density functional approximations, J. Chem. Phys. 105 (1996) 9982–9985, doi:10.1063/1.472933.
[76] W. Humphrey, A. Dalke, K. Schulten, VMD:visual molecular dynamics, J. Mol. Graph. 14 (1) (1996) 33–38, doi:10.1016/0263-7855(96)00018-5.